ADVANCES IN MANUFACTURING SCIENCE AND TECHNOLOGY
Vol. 41, No. 2, 2017
DOI: 10.2478/amst-2017-0009

MATHEMATICAL MODEL OF TOOTH FLANK OF WORM WHEEL WITH ARC PROFILE IN GLOBOID WORM GEAR

Piotr Połowniak

S u m m a r y

This paper presents a mathematical description of tooth flank surface of the worm wheel generated by the hourglass worm with convex or concave tooth axial profile. The kinematic system of globoid worm gear and tooth formation of worm wheel was performed. The mathematical description of tooth flank of globoid worm with arc profile was used. The presented mathematical model of tooth flank of worm wheel with mathematical model of hourglass worm can be used to analyze e.g. the contact pattern of the gear.

Keywords: globoid worm gear, worm wheel

Matematyczny model boku zęba ślimacznicy o zarysie łukowym przekładni ślimakowej globoidalnej

S t r e s z c z e n i e

Przedstawiono w pracy matematyczny opis powierzchni boku zęba ślimacznicy kształtowanego globoidalnym frezem ślimakowym o zarysie wklęsłym lub wypukłym. Omówiono układ kinematyczny przekładni ślimakowej globoidalnej i kształtowania boku zęba ślimacznicy. Stosowano matematyczny opis powierzchni bocznej ślimaka globoidalnego o zarysie łukowym. Przyjęty matematyczny model boku zęba ślimacznicy o zarysie łukowym wraz z modelem matematycznym ślimaka globoidalnego będzie podstawą analizy m.in. śladu styku przekładni.

Słowa kluczowe: przekładnia ślimakowa globoidalna, ślimacznica

1. Introduction

Globoid worm drive was initially invented approximately in 1765 by H. Hindley [1, 2]. In the beginning of XX century, Samuel I. Cone patented the applicable technology to manufacture this worm drive [3, 4]. In this case the hourglass worm is lathed by a lathe tool with straight blade. The meshing worm wheel is generated by an hourglass hob similar to the hourglass worm. Because of advantages of this kind of drive, it achieved wide application rapidly. This gear drive has the increased load capacity due to the higher contact ratio in comparison with that of conventional worm gear drives, higher efficiency results

Address: Piotr POŁOWNIAK, MSc Eng., Rzeszow University of Technology, Department of Mechanical Engineering, 8 Powstańców Warszawy Ave., 35-959 Rzeszów, e-mail: ppolowniak@prz.edu.pl

from the existence of more favorable lubrication conditions. The special shape of the worm increases the number of teeth that are simultaneously in mesh and improves the conditions of force transmission. The conditions of lubrication and the efficiency of the invented drive (in comparison with a worm gear drive with a cylindrical worm) are substantially better [1, 2, 5]. The complex geometry of the globoid worm gear drive and its advantages inspired many researchers to develop the analytical aspects of the meshing of the worm and the worm gear tooth surfaces. Researchers proposed novel worm drives, like Wildhaber worm drive [6], where the hourglass worm is generated by the normal plane worm gear. The other example is involute globoid worm drive. In this case the gear consists with an involute gear and an hourglass worm generated by the involute gear. The novel type of this kind of involute gear is the involute beveloid gear enveloping hourglass worm. This drive is consisted of an involute beveloid gear and an hourglass worm generated by the involute beveloid gear surface. The next type is non-backlash double-roller enveloping hourglass worm drive and the tori double-enveloping hourglass worm drive. Generally globoid worm drives are widely used in various industrial sections nowadays [7].

The new type of globoid worm gear consists of hourglass worm with convex or concave tooth axial profile and worm wheel is proposed. The mathematical description of tooth flank of worm with arc profile was presented in [8]. The aim of this work is to describe the tooth flank of worm wheel, which is generated by the hourglass worm with convex or concave tooth axial profile. The mathematical model of worm and presented worm wheel can be used to analyze e.g. contact region of such kind of gear.

2. Kinematic coordinate system of globoid worm gear

The kinematic coordinate system of globoid worm gear is shown in Fig. 1.

The globoid worm gear is crossed gear with angle of 90°. The two stationary coordinate system S_1 $(x_1 y_1 z_1)$ and S_2 $(x_2 y_2 z_2)$ connected with worm and worm wheel respectively were established. These systems can be handled as systems associated with housing. The moveable coordinate system S_1' $(x_1' y_1' z_1')$ of worm and S_2' $(x_2' y_2' z_2')$ of worm wheel was introduced. Centers of coordinate systems are described as O_1 and O_2. The distance between centers a is also the distance between the centers of coordinate systems. Worm rotates clockwise about z_1' axis by the angle φ_1. Then worm wheel rotates clockwise about x_2' by the angle φ_2 (in case of lead left worm). φ_1 and φ_2 are also the geometric surface parameters. Between φ_1 and φ_2 exists relationship resulting from gear ratio. The gear ratio i is defined as ratio of number of teeth on the worm to number of teeth on worm wheel. This gives:

$$i = \frac{z_1}{z_2} = \frac{\varphi_2}{\varphi_1} \tag{1}$$

where: z_1 – number of teeth on worm, z_2 – number of teeth on worm wheel, φ_1 – worm rotation parameter and the main surface parameter, φ_2 – worm wheel rotation parameter and the auxiliary surface parameter.

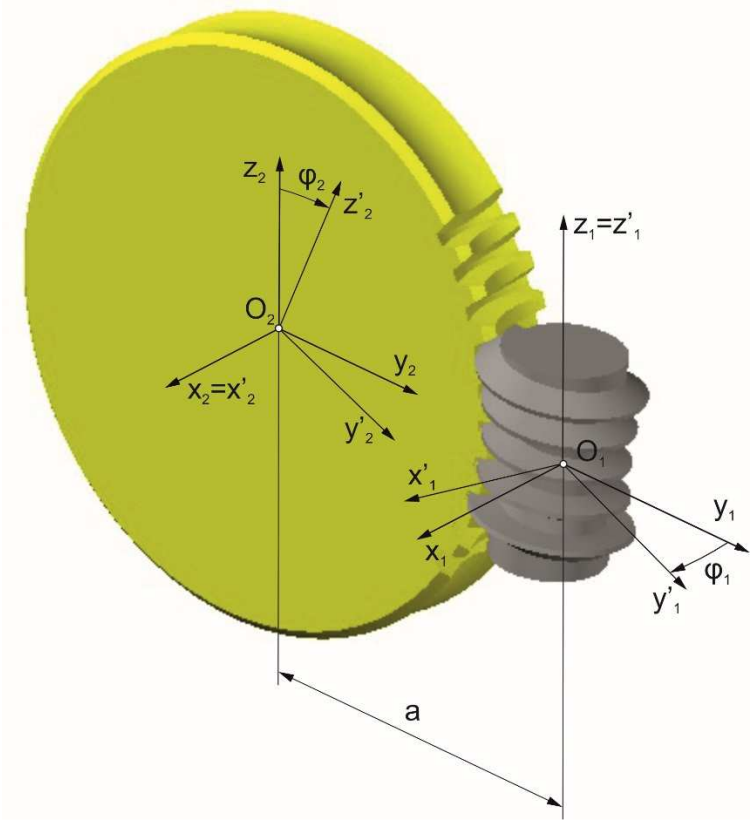

Fig. 1. Kinematic coordinate system of globoid worm gear

The surface of worm Σ_1 in coordinate system $x_1'y_1'z_1'$ is represented by a position vector $\bar{r}_1^{(1')}$. Similarly, the surface of worm wheel Σ_2 in the $x_2'y_2'z_2'$ coordinate system is represented by position vector $\bar{r}_2^{(2')}$. To describe the geometrical model of the teeth and mesh of the worm and worm gear, it is necessary to show the transformations between the systems using a homogeneous matrix of 4 × 4, which contains a rotation matrix and an offset vector.

$$M_{11'} = \begin{bmatrix} \cos(\varphi_1) & -\sin(\varphi_1) & 0 & 0 \\ \sin(\varphi_1) & \cos(\varphi_1) & 0 & 0 \\ 0 & 0 & 1 & 0 \\ 0 & 0 & 0 & 1 \end{bmatrix} \tag{2}$$

$$M_{21} = \begin{bmatrix} 1 & 0 & 0 & 0 \\ 0 & 1 & 0 & a \\ 0 & 0 & 1 & 0 \\ 0 & 0 & 0 & 1 \end{bmatrix} \tag{3}$$

$$M_{22'} = \begin{bmatrix} 1 & 0 & 0 & 0 \\ 0 & \cos(\varphi_2) & -\sin(\varphi_2) & 0 \\ 0 & \sin(\varphi_2) & \cos(\varphi_2) & 0 \\ 0 & 0 & 0 & 1 \end{bmatrix} \tag{4}$$

$$M_{12} = \begin{bmatrix} 1 & 0 & 0 & 0 \\ 0 & 1 & 0 & -a \\ 0 & 0 & 1 & 0 \\ 0 & 0 & 0 & 1 \end{bmatrix} \tag{5}$$

$$M_{1'1} = \begin{bmatrix} \cos(-\varphi_1) & -\sin(-\varphi_1) & 0 & 0 \\ \sin(-\varphi_1) & \cos(-\varphi_1) & 0 & 0 \\ 0 & 0 & 1 & 0 \\ 0 & 0 & 0 & 1 \end{bmatrix} \tag{6}$$

$$M_{2'2} = \begin{bmatrix} 1 & 0 & 0 & 0 \\ 0 & \cos(-\varphi_2) & -\sin(-\varphi_2) & 0 \\ 0 & \sin(-\varphi_2) & \cos(-\varphi_2) & 0 \\ 0 & 0 & 0 & 1 \end{bmatrix} \tag{7}$$

where: $M_{11'}$ – is the homogeneous matrix of transformation from $1'$ to 1, M_{21} – is the homogeneous matrix of transformation from 1 to 2, $M_{22'}$ is the homogeneous matrix of transformation from $2'$ to 2, M_{12} – is the homogeneous matrix of transformation from 2 to 1, $M_{1'1}$ – is the homogeneous matrix of transformation from 1 to $1'$, $M_{2'2}$ – is the homogeneous matrix of transformation from 2 to $2'$.

3. Mathematical model of hourglass worm with arc profile

Mathematical model of hourglass single lead left worm with arc profile in axis section was particularly described in [8]. It is necessary to recall the equation of the tooth flank of worm:

$$\bar{r}_1^{(1')} = \begin{bmatrix} \mathrm{x}_1(\theta)\cdot\cos(\varphi_1) - \mathrm{a}\cdot\sin(\varphi_1) + \mathrm{a}\cdot\cos(\varphi_2)\cdot\sin(\varphi_1) + \\ +y_1(\theta)\cdot\cos(\varphi_2)\cdot\sin(\varphi_1) - z_1(\theta)\cdot\sin(\varphi_2)\cdot\sin(\varphi_1) \\ -\mathrm{x}_1(\theta)\cdot\sin(\varphi_1) - \mathrm{a}\cdot\cos(\varphi_1) + \mathrm{a}\cdot\cos(\varphi_1)\cdot\cos(\varphi_2) + \\ +y_1(\theta)\cdot\cos(\varphi_2)\cdot\cos(\varphi_1) - z_1(\theta)\cdot\sin(\varphi_2)\cdot\cos(\varphi_1) \\ \mathrm{a}\cdot\sin(\varphi_2) + y_1(\theta)\cdot\sin(\varphi_2) + z_1(\theta)\cdot\cos(\varphi_2) \\ 1 \end{bmatrix} \quad (8)$$

where: φ_1 – worm surface parameter, $x_1(\theta)$, $y_1(\theta)$, $z_1(\theta)$ are the parametric equation of axial section profile of worm tooth. They can be expressed in $y_1 z_1$ plane as:

$$\begin{aligned} x_1(\theta) &= 0 \\ y_1(\theta) &= R\cdot\cos(\theta) + y_0 \\ z_1(\theta) &= R\cdot\sin(\theta) + z_0 \end{aligned} \quad (9)$$

where: θ – parameter of profile (range of arc profile: $\theta_p \le \theta \le \theta_k$), y_0, z_0 – coordinates of arc center, R – radius of arc [8].

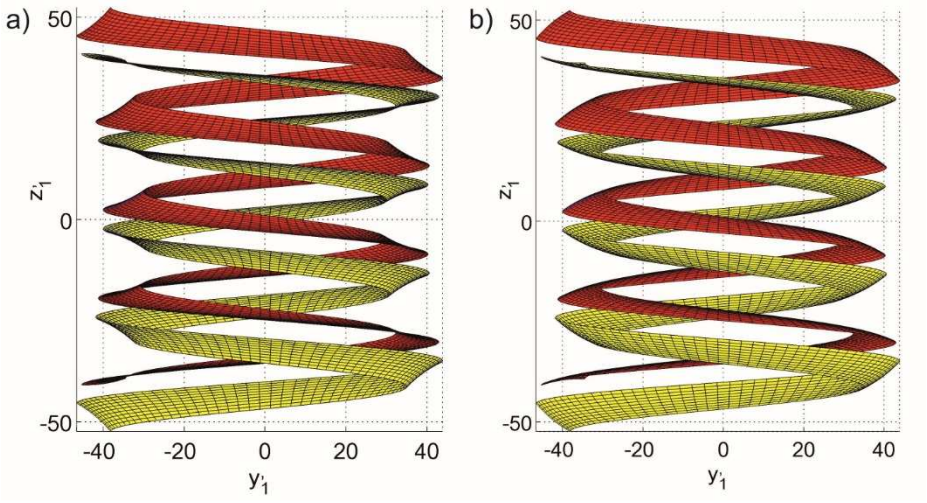

Fig. 2. Tooth sides of globoid worm with: a) concave profile, b) convex profile, based on [8]

To obtain convex or concave worm surface is necessary to substitute in eq. (9) the proper coordinates of arc center and range of arc profile, what was described in [8]. Figure 2 shows the both tooth surface of convex and concave globoid worm created on the grounds of eq. (8).

4. Mathematical model of worm gear formed by tool with arc profile

The kinematic cutting system of worm wheel is the same like system shown in Fig. 1. The description of one side of the tooth surface is presented. It is enough to make afterwards for example the analysis of contact pattern. The worm wheel tooth surface is formed by a surface of worm hob tooth. It is noted that worm wheel surface is divided into three regions (Fig. 3) [5, 9]. Region II is the envelope of the family of contact lines of gear set. Region I and III is formed by a first cutting edge of worm hob cutter (Fig. 4). One extreme cutting edge of worm hob cutter forms one side of worm wheel tooth and the second edge the another flank.

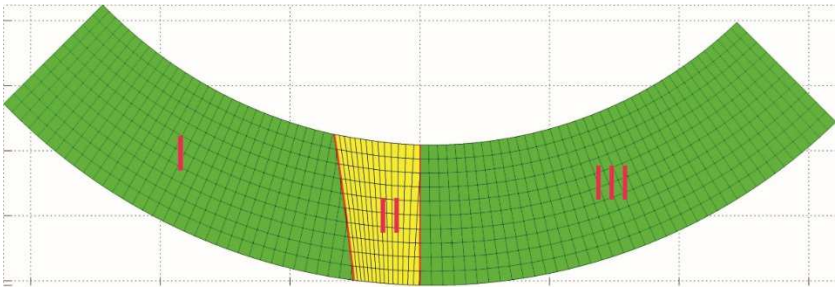

Fig. 3. Explanation view of tooth side of globoid worm wheel

The condition of existence of an envelope is represented by the equation of meshing:

$$n_x v_x + n_y v_y + n_z v_z = 0 \tag{10}$$

where: n_x, n_y, n_z – components of the normal vector to the surface, v_x, v_y, v_z – components of the tangent vector.

Relation between rotation of worm wheel φ_2 to rotation of worm φ_1 is given as:

$$M_{2'1'} = M_{2'2} \cdot M_{21} \cdot M_{11'} \tag{11}$$

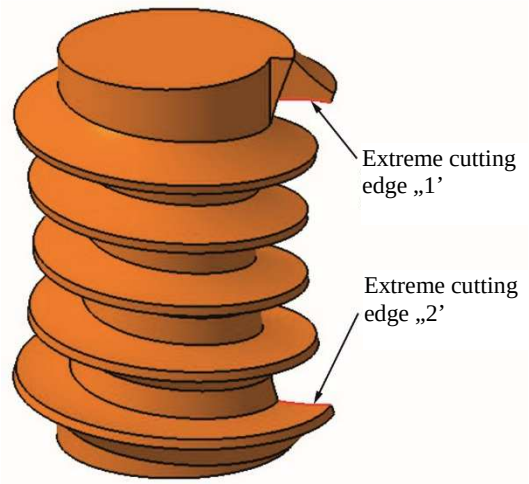

Fig. 4. Illustrative figure of worm hob model with marked cutting edges generating a part of tooth side of worm wheel

Substituting eq. (2), (3), (7) to eq. (11) the expression (12) is obtained:

$$M_{2'1'} = \begin{bmatrix} \cos(\varphi_1) & -\sin(\varphi_1) & 0 & 0 \\ \cos(\varphi_2)\sin(\varphi_1) & \cos(\varphi_2)\cdot\cos(\varphi_1) & \sin(\varphi_2) & \mathrm{a}\cdot\cos(\varphi_2) \\ -\sin(\varphi_1)\sin(\varphi_2) & -\cos(\varphi_1)\sin(\varphi_2) & \cos(\varphi_2) & -\mathrm{a}\cdot\sin(\varphi_2) \\ 0 & 0 & 0 & 1 \end{bmatrix} \tag{12}$$

The surface normal vector $\bar{n}_1^{(2')}$ is expressed as:

$$\bar{n}_1^{(2')} = \begin{bmatrix} n_{x1}^{(2')} \\ n_{y1}^{(2')} \\ n_{z1}^{(2')} \end{bmatrix} = L_{2'1'} \cdot \left(\frac{\partial \bar{r}_1^{(1')}}{\partial \varphi_1} \times \frac{\partial \bar{r}_1^{(1')}}{\partial \theta}\right) \tag{13}$$

where: $L_{2'1'}$ – is the matrix of transformation from $1'$ do $2'$. $L_{2'1'}$ can be obtained by crossing out the last row and the last column of the homogeneous matrix of transformation:

$$L_{2'1'} = \begin{bmatrix} \cos(\varphi_1) & -\sin(\varphi_1) & 0 \\ \cos(\varphi_2)\cdot\sin(\varphi_1) & \cos(\varphi_2)\cdot\cos(\varphi_1) & \sin(\varphi_2) \\ -\sin(\varphi_1)\sin(\varphi_2) & -\cos(\varphi_1)\sin(\varphi_2) & \cos(\varphi_2) \end{bmatrix} \tag{14}$$

Derivative $\frac{\partial \bar{r}_1^{(1')}}{\partial \varphi_1}$ is expressed as:

$$\frac{\partial \bar{r}_1^{(1')}}{\partial \varphi_1} =$$

$$= \begin{bmatrix} -x_1(\theta)\cdot\sin(\varphi_1) - a\cdot\cos(\varphi_1) + a\cdot\cos(\varphi_2)\cdot\cos(\varphi_1) + y_1(\theta)\cdot\cos(\varphi_2)\cdot\cos(\varphi_1) - \\ -z_1(\theta)\cdot\sin(\varphi_2)\cdot\cos(\varphi_1) - \mathrm{i}\cdot a\cdot\sin(\varphi_2)\cdot\sin(\varphi_1) - \\ -\mathrm{i}\cdot y_1(\theta)\cdot\sin(\varphi_2)\cdot\sin(\varphi_1) - \mathrm{i}\cdot z_1(\theta)\cdot\cos(\varphi_2)\cdot\sin(\varphi_1) \\ \\ -x_1(\theta)\cdot\cos(\varphi_1) + \mathrm{a}\cdot\sin(\varphi_1) - \mathrm{a}\cdot\cos(\varphi_2)\cdot\sin(\varphi_1) - y_1(\theta)\cdot\cos(\varphi_2)\cdot\sin(\varphi_1) + \\ +z_1(\theta)\cdot\sin(\varphi_2)\cdot\sin(\varphi_1) - \mathrm{i}\cdot a\cdot\sin(\varphi_2)\cdot\cos(\varphi_1) - \\ -\mathrm{i}\cdot y_1(\theta)\cdot\sin(\varphi_2)\cdot\cos(\varphi_1) - i\cdot z_1(\theta)\cdot\cos(\varphi_2)\cdot\cos(\varphi_1) \\ \\ a\cdot i\cdot\cos(\varphi_2) + \mathrm{i}\cdot y_1(\theta)\cdot\sin(\varphi_2) - \mathrm{i}\cdot z_1(\theta)\cdot\sin(\varphi_2) \end{bmatrix}$$

(15)

The expression $\frac{\partial \bar{r}_1^{(1')}}{\partial \theta}$ is solved by substituting for $x_1(\theta)$, $y_1(\theta)$ and $z_1(\theta)$ the parametric equation (9) of axial section profile of worm tooth. Derivative $\frac{\partial \bar{r}_1^{(1')}}{\partial \theta}$ is expressed as:

$$\frac{\partial \bar{r}_1^{(1')}}{\partial \theta} = \begin{bmatrix} -\mathrm{R}\cdot\cos(\varphi_2)\cdot\sin(\varphi_1)\cdot\sin(\theta) - \mathrm{R}\cdot\cos(\theta)\cdot\sin(\varphi_1)\cdot\sin(\varphi_2) \\ -\mathrm{R}\cdot\cos(\varphi_1)\cdot\cos(\varphi_2)\cdot\sin(\theta) - \mathrm{R}\cdot\cos(\varphi_1)\cdot\cos(\theta)\cdot\sin(\varphi_2) \\ \mathrm{R}\cdot\cos(\varphi_2)\cdot\cos(\theta) - \mathrm{R}\cdot\sin(\varphi_2)\cdot\sin(\theta) \end{bmatrix} \tag{16}$$

The surface normal vector $\bar{n}_1^{(2')}$ is obtained, substituting eq. (14), (15), (16) into expression (13). The explicit representation of $\bar{n}_1^{(2')}$ is not presented due to its complexity.

Tangent vector can be calculated based on kinematics of worm gear. It is obtained by applying the following equation:

$$\bar{v}_1^{(2')} = \begin{bmatrix} v_{x1}^{(2)} \\ v_{y1}^{(2')} \\ v_{z1}^{(2')} \end{bmatrix} = \frac{d\bar{r}_1^{(2')}}{d\varphi_2} = \frac{dM_{2'1'}}{d\varphi_2}\cdot\bar{r}_1^{(1')} \tag{17}$$

The derivative $\frac{\mathrm{d}M_{2'1'}}{\mathrm{d}\varphi_2}$ is calculated substituting in (12) for $\varphi_1 = \frac{\varphi_2}{i}$. It yields:

$$\frac{\mathrm{d}M_{2'1'}}{\mathrm{d}\varphi_2} = \begin{bmatrix} a_{11} & a_{12} & a_{13} & a_{14} \\ a_{21} & a_{22} & a_{23} & a_{24} \\ a_{31} & a_{32} & a_{33} & a_{34} \\ a_{41} & a_{42} & a_{43} & a_{44} \end{bmatrix} \tag{18}$$

where:

$$a_{11} = -\frac{\sin(\varphi_1)}{i},$$
$$a_{12} = -\frac{\cos(\varphi_1)}{i},$$
$$a_{21} = \frac{1}{\mathrm{i}} \cdot \cos(\varphi_1)\cos(\varphi_2) - \sin(\varphi_1)\sin(\varphi_2),$$
$$a_{22} = -\cos(\varphi_1) \cdot \sin(\varphi_2) - \frac{1}{i} \cdot \sin(\varphi_1)\cos(\varphi_2),$$
$$a_{23} = \cos(\varphi_2),$$
$$a_{24} = -\mathrm{a} \cdot \sin(\varphi_2),$$
$$a_{31} = -\frac{1}{i} \cdot \cos(\varphi_1)\sin(\varphi_2) - \sin(\varphi_1)\cos(\varphi_2),$$
$$a_{32} = -\cos(\varphi_1) \cdot \cos(\varphi_2) + \frac{1}{i} \cdot \sin(\varphi_1)\sin(\varphi_2),$$
$$a_{33} = -\sin(\varphi_2),$$
$$a_{34} = -\mathrm{a} \cdot \cos(\varphi_2),$$
$$a_{13} = a_{14} = a_{41} = a_{42} = a_{43} = 0,$$
$$a_{44} = 1.$$

Eq. (8) and (18) are substituted into (17). The explicit representation of $\bar{v}_1^{(2')}$ is not presented due to its complexity. In the general equation of gear meshing the eq. of surface normal vector $\bar{n}_1^{(2')}$ and tangent vector $\bar{v}_1^{(2')}$ are introduced:

$$\bar{n}_1^{(2')} \cdot \bar{v}_1^{(2')} = \begin{bmatrix} n_{x1}^{(2')} \\ n_{y1}^{(2')} \\ n_{z1}^{(2')} \end{bmatrix} \cdot \begin{bmatrix} v_{x1}^{(2')} \\ v_{y1}^{(2')} \\ v_{z1}^{(2')} \end{bmatrix} = 0 \tag{19}$$

After solving the eq. (19), for given parameters θ the solutions set of φ_1 is obtained. These parameters define contact line between worm and worm wheel. Substituting the solutions to eq. (8) contact lines in S_1' coordinate system are received:

$$\bar{r}_{cl}^{(1')} = \bar{r}_{1}^{(1')}(\varphi_1, \theta) \tag{20}$$

where: $\bar{r}_{cl}^{(1')}$ – vector of contact line, φ_1, θ – parameters satisfying the eq. (19).

Contact lines on the tooth side of worm with concave (Fig. 5) and convex (Fig. 6) tooth profile are plotted.

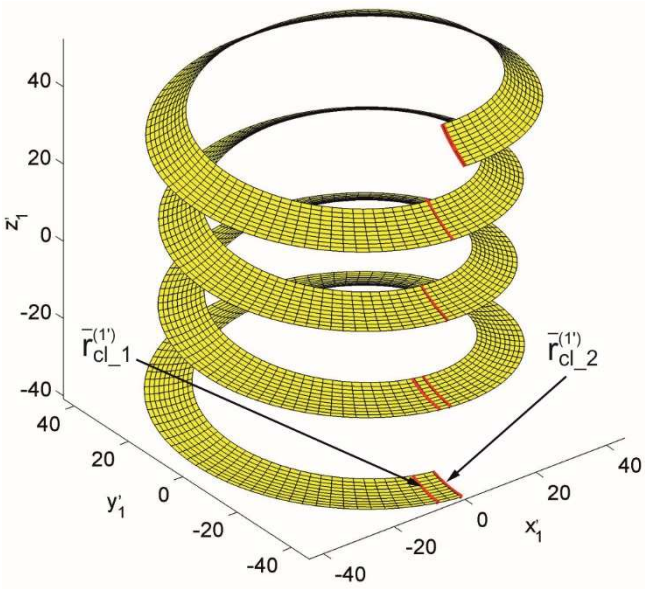

Fig. 5. Contact lines shown in S_1' coordinate system (tool with concave profile)

Surface Σ_1 is in tangent with Σ_2 at every instant of two lines. One line lies in the middle plane of worm gear. While the worm is in mesh with worm wheel, the character of these generated lines, lying in the plane $y_1'z_1'$, is constant. The profile of these lines is concave or convex depends of worm tooth profile. The other contact lines between worm surface and worm wheel surface are the envelope to the family of Σ_1. These lines generate that part of worm wheel, which is described as region II. Region II ($\bar{r}_{2\_Region\_II}^{(1')}$) can be obtained by rotating the worm with specified value in rotation range from 0 to 2π and determining the contact lines. Those lines are selected, which are not lying in the axial section of worm (or in middle plane of worm gear). Then the selected contact lines should be brought to the one tooth side of worm wheel, as shown as example in Fig. 7.

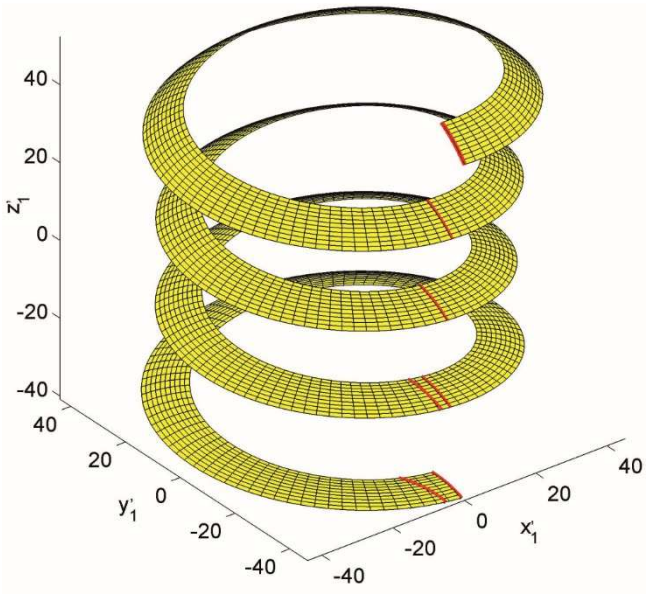

Fig. 6. Contact lines shown in S_1' coordinate system (tool with convex profile)

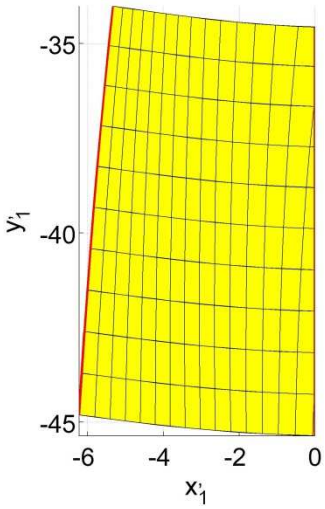

Fig. 7. Region II of that part worm wheel which is envelope to the family of worm presented in S_1' coordinate system (here region II generated by the tool with concave profile)

Region I and III is formed by a first cutting edge of worm hob cutter. It is equivalent with the extreme contact line, lying in the $y_1'z_1'$ plane. The alternative is a transformation of axial profile of worm $\bar{r}^{(1')}_{1(\varphi_1=\varphi_{1p})}$ using the eq. (8). It is assumed that the extreme cutting edge of the tool lies in the plane $y_1'z_1'$, like in Fig. 5 or 6. Otherwise it is necessary to rotate the tool by an angle to ensure, that this condition is met.

The surface generated by the extreme cutting edge represented in coordinate system of worm S_1' is obtained by applying the following equation:

$$\bar{r}_2^{*(1')} = M_{1'1} \cdot M_{12} \cdot M_{2'2} \cdot M_{21} \cdot \bar{r}^{(1')}_{1(\varphi_1=\varphi_{1p})} \tag{21}$$

In eq. (21) in the matrices the range of parameter φ_1 is selected to obtain the worm wheel tooth surface of a given width ($\varphi_{1p} \leq \varphi_1 \leq \varphi_{1k}$). In the Fig. 8 the tooth surface of worm wheel generated by extreme cutting edge is plotted.

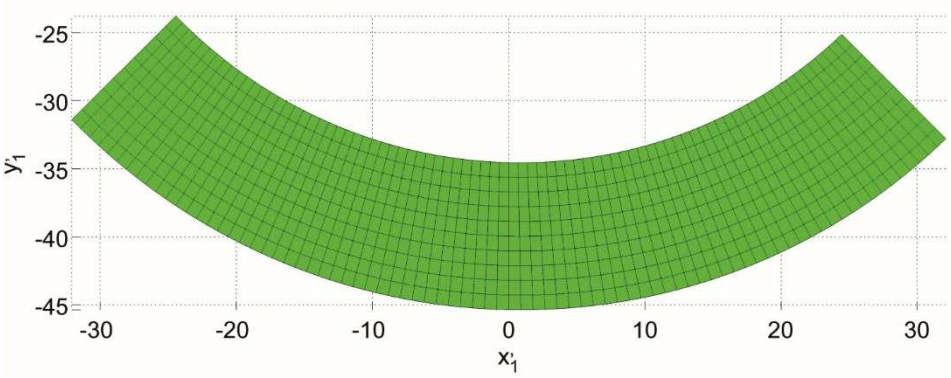

Fig. 8. Surface of worm wheel tooth generated by extreme cutting edge

From the surface shown in Fig. 8 region I and III have to be separated. The two contact lines in the area of the extreme cutting edge of the tool are the boundaries of the regions (Fig. 5). For region I is the contact line, which doesn't lie in the axial plane of tool ($\bar{r}^{(1')}_{cl\_1}$ marked in Fig. 5). For region III is the contact line lying in the axial plane ($\bar{r}^{(1')}_{cl\_2}$ marked in Fig. 5). Figure 9 shows the separated region I and III of the worm wheel tooth surface generated during machining through the extreme cutting edge of the tool.

The tooth surface of worm wheel is generated by the combination of the regions I, II, III:

$$\bar{r}_2^{(1')} = \bar{r}_{2\_Region\_I}^{(1')} \cup \bar{r}_{2\_Region\_II}^{(1')} \cup \bar{r}_{2\_Region\_III}^{(1')} \tag{22}$$

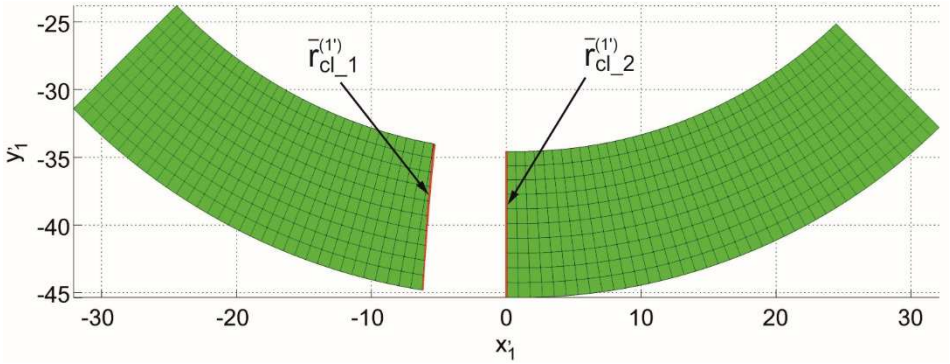

Fig. 9. The separated region I and III of the worm wheel tooth surface generated during machining through the extreme edge of the tool (here generated by the tool with concave profile)

The worm wheel tooth surface formed by a tool with concave tooth profile is shown in Fig. 10.

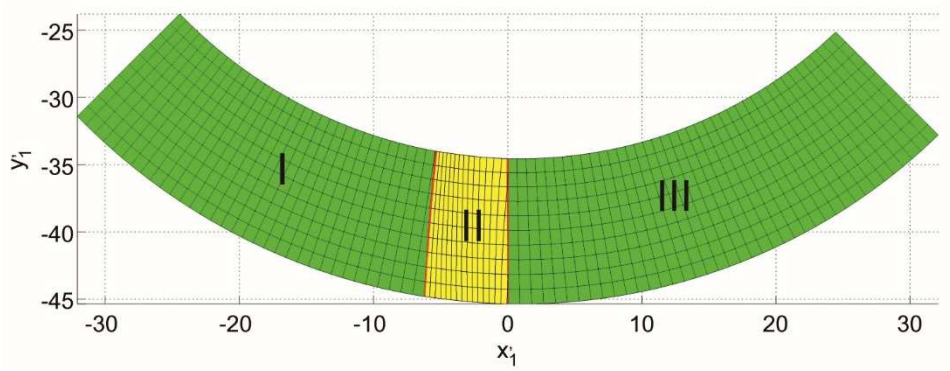

Fig. 10. The worm wheel tooth surface of globoid worm gear generated by the tool with concave profile

Figure 11 shows the worm wheel tooth surface formed by a tool with convex tooth profile.

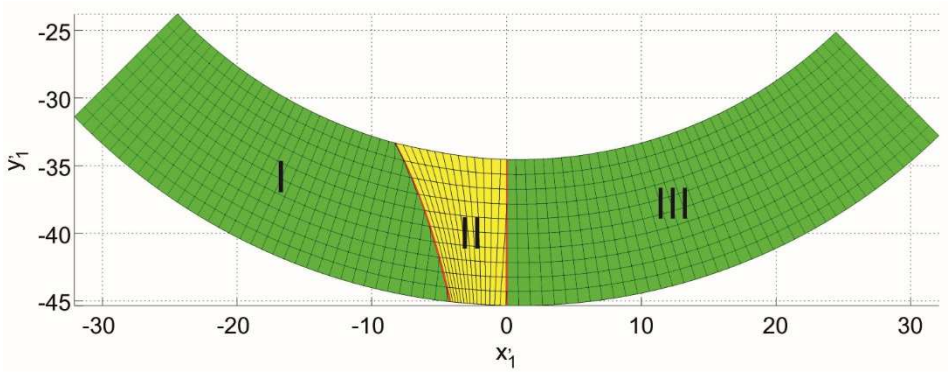

Fig. 11. The worm wheel tooth surface of globoid worm gear generated by the tool with convex profile

Conclusion

Presented mathematical model of tooth flank surface of worm wheel generated by a globoid worm hob with arc profile shows that its determination is complex. The character of the contact lines between worm and worm wheel depends on the type of tooth profile of worm. The shape of contact lines for concave or convex worm tooth profile can have the significant influence for lubrication conditions. The extreme cutting edge of worm hob has a considerable impact by generating the tooth side of worm wheel. It is circa 85% of tooth width of worm wheel. The presented mathematical model of tooth flank of worm wheel with mathematical model of worm tooth can be used to analyze e.g. the contact pattern of the gear.

References

[1] I. DUDAS: The theory and practice of worm gear drives. Penton Press, London 2000.
[2] F.L. LITVIN: Development of Gear Technology and Theory of Gearing. NASA, Levis Research Center 1999.
[3] S.I. CONE: Globoidal hob. U.S. Pat. No. 2026215 A.
[4] S.I. CONE: Method of and apparatus for cutting worm gearing. U.S. Pat. No. 1885686 A.
[5] F.L. LITVIN, A. FUENTES: Gear Geometry and Applied Theory. Cambridge University Press, Cambridge 2004.

[6] E. WILDHABER: Wildhaber worm drive. U.S. Pat. No. 3386305, 1966.
[7] Y.H. CHEN, Y. CHEN, W. LUO, G. ZHANG: Development and Classification of Worm Drive. Proceedings of the 14th IFToMM World Congress. Taipei 2015.
[8] P. POŁOWNIAK, M. SOBOLAK: Matematyczny model ślimaka globoidalnego o wklęsłym i wypukłym zarysie zęba. *Mechanik*, **90**(2017)1, 6-7.
[9] P. POŁOWNIAK, M. SOBOLAK: Wpływ skrajnej krawędzi frezu ślimakowego na kształtowanie boku zęba ślimacznicy przekładni ślimakowej globoidalnej. *Mechanik*, **89**(2016)7, 625-627.

Received in December 2016